PHYSICAL REVIEW D **83,** 114043 (2011)

Next-to-leading order QCD corrections for W^+W^- pair production in association with two jets at hadron colliders

Tom Melia*
Rudolf Peierls Centre for Theoretical Physics, 1 Keble Road, University of Oxford, United Kingdom

Kirill Melnikov†
Department of Physics and Astronomy, Johns Hopkins University, Baltimore, Maryland 21218, USA

Raoul Röntsch‡
Rudolf Peierls Centre for Theoretical Physics, 1 Keble Road, University of Oxford, United Kingdom

Giulia Zanderighi§
Rudolf Peierls Centre for Theoretical Physics, 1 Keble Road, University of Oxford, United Kingdom
(Received 24 April 2011; published 22 June 2011)

We compute the NLO QCD corrections to the pair production of W-bosons in association with two jets at the Tevatron and the LHC. This process is an important background to heavy Higgs-boson production in association with two jets, either in gluon or weak boson fusion. We consider leptonic decays of W-bosons and include all the spin correlations exactly. For natural choices of the renormalization scale, the NLO QCD corrections to $pp(\bar{p}) \to W^+W^-jj$ are moderate but different for various values of the center-of-mass collision energy at the LHC and the Tevatron, emphasizing the need to compute them explicitly.

DOI: 10.1103/PhysRevD.83.114043 PACS numbers: 12.38.Bx, 14.65.Ha

I. INTRODUCTION

The Large Hadron Collider (LHC) has begun to explore the standard model (SM) of particle physics in a new energy regime and will in time gather more data than any previous hadron collider experiment. To further our understanding of the SM and as to what may lie beyond it, we attempt to describe outcomes of proton collisions in sufficient detail, for comparison with the observed data. An accurate knowledge of SM processes is particularly important as their cross sections are often much larger than those for many interesting New Physics processes. Unless physics beyond the SM presents itself in a stark way, disentangling it from SM backgrounds will require an accurate description of the latter. Parton level calculations at leading order (LO) in the strong coupling constant are often insufficient for this purpose. They exhibit a strong unphysical dependence on factorization and renormalization scales, leading to large uncertainties in the predictions. Data-driven estimates of the backgrounds are also subject to large uncertainties if they rely on LO theoretical predictions: here the idea is to determine the normalization of the LO cross section for a given background process in a region essentially free from any New Physics signal. Once the LO is ''validated'' using data, one extrapolates it to the region of interest. It is clear that such a procedure can only work if higher-order QCD corrections are uniform over phase space, which is not guaranteed in general. As follows from many successful analyses at the Tevatron, a good way to reduce the uncertainty is to extend the theoretical description of a given process to next-to-leading-order (NLO) in perturbative QCD.

The past five years have seen an extraordinary progress in the development of methods that are suitable to deal with NLO QCD computations for high-multiplicity processes. Refinements of traditional computational techniques based on the Passarino-Veltman reduction of tensor integrals led to the development of highly efficient, Feynman-diagram-based technology for NLO QCD computations [1–3]. At the same time, new techniques based on unitarity and on-shell methods [4–10] sufficiently matured to become relevant for practical applications. As a result, a large number of $2 \to 4$ processes were studied at NLO in QCD in the past two years. The list includes $pp \to W(Z, \gamma) + 3$ jets [11–16], $pp \to t\bar{t}b\bar{b}$ [17–19], $pp \to t\bar{t} +$ 2 jets [20], $pp \to b\bar{b}b\bar{b}$ [21], $pp \to t\bar{t} \to W^+W^-b\bar{b}$ [22,23], and $pp \to W^+W^+ + 2$ jets [24]. This last process has been implemented recently in POWHEG-BOX [25]. This combines NLO accuracy with a parton shower detailed description of the final state.

The first $2 \to 5$ process, $pp \to W + 4$ jets, has also been computed recently through NLO QCD using on-shell methods [26]. Some groups also started employing those advances with the intention of developing a platform for fully automated NLO QCD calculation [27,28].

The goal of this paper is to study the production of a pair of W-bosons in association with two jets in hadron

*t.melia1@physics.ox.ac.uk
†melnikov@pha.jhu.edu
‡r.rontsch1@physics.ox.ac.uk
§g.zanderighi1@physics.ox.ac.uk

collisions, including the NLO QCD corrections. The production of a W-boson pair in association with zero, one or two jets is an important background to searches for intermediate and heavy Higgs boson, where the decay $H \to W^+W^-$ opens up. At the Tevatron, searches for intermediate-mass Higgs bosons treat processes $p\bar{p} \to H + n$ jets, $n = 0, 1, \geq 2$ separately, because dominant backgrounds depend on the number of identified jets in the final state (see e.g. [29]). While most of the sensitivity in Higgs-boson searches comes from the process with the largest cross section, $p\bar{p} \to H + 0$ jets, the production of the Higgs boson in association with two jets is also relevant [30,31]. Because $p\bar{p} \to W^+W^-jj$ is an irreducible background to the Higgs-boson production in association with two jets, it is important to have NLO QCD predictions for this process.

There is yet another reason to want an improved description of W^+W^-jj production in hadron collisions. At the LHC the Higgs boson can be produced with a sizable cross section in weak boson fusion (WBF) [30,32]. In addition to the Higgs-boson decay products which, as we assume, are pairs of W-bosons, the signature of the process involves two forward tagging jets. In this case, $pp \to W^+W^-jj$ is the irreducible background. The Higgs-production cross section in WBF is known through NLO QCD [32–34], and it is desirable for the dominant background process to be known to the same order in perturbative QCD as well.

Finally, we note that jets, charged leptons and missing energy is one of the classic signatures of dark-matter-type processes at colliders. In such scenarios the missing energy appears due to the dark-matter candidate escaping the detector. The process $pp \to W^+W^-jj$ is a SM background with a similar signature, where leptonic decays of W-bosons lead to invisible neutrinos.

Several studies in the past decade addressed the production of W-boson pairs in hadron collisions, including NLO QCD corrections. In particular, $pp \to W^+W^-$ with no jets was studied in Refs. [35–38]. The production of a pair of W-bosons in association with one jet including decays to leptons was studied through NLO QCD in Refs. [39,40]. In both cases, for the choice of the renormalization and factorization scales $\mu = M_W$, QCD corrections were found to be significant, of the order of (25–50)%. These results further motivate the need to understand the production of W^+W^- in association with two or even more jets at NLO in QCD.

In this paper we allow for leptonic decays of the W-pair including all spin correlations. Dilepton final states are the ones that are relevant for ongoing Higgs searches at the Tevatron and, in general, these final states provide the cleanest signature to identify the production of W-bosons at a hadron collider. For this reason, we find it reasonable to focus on these states only.

We remind the reader that the branching fraction for the W-boson to decay to a definite-flavor lepton final state is about 10%. Since we have two W-bosons decaying leptonically, we get a hit by a factor $\mathcal{O}(10^{-2})$ when the cross section for the dilepton final state is compared with the cross section for stable W-bosons. It is therefore amazing that the cross section for the process $pp \to (W^+ \to \nu_\mu \mu^+) + (W^- \to e^- \bar{\nu}_e) + jj$ is still reasonably large. In particular, we find that the cross section for the LHC running at an energy of 7 TeV is around 40 fb, which means that a few of these events should have already been seen at this collider at the time of publication, and quite a significant number of such events should be produced at the LHC by the end of the next year. The cross section further increases to about 0.14 pb at 14 TeV, so there is no doubt that the experimental study of this process is feasible. Even at the Tevatron, where the cross section with the "Higgs-like" cuts for one flavor assignment is just 2.0 fb, assuming 50% efficiency, about 40 $e^+e^-\bar{\nu}\nu jj$, $\mu^+\mu^-\bar{\nu}\nu jj$, $\mu^+e^-\bar{\nu}\nu jj$, $e^+\mu^-\bar{\nu}\nu jj$ events should have been recorded already.

The computation of NLO QCD corrections to hadroproduction of W^+W^-, in association with two jets, is also interesting from the point of view of further developing on-shell methods for one-loop computations. Recall that, as currently formulated, on-shell methods require ordering of external lines which is achieved by working with color-ordered [41] or primitive amplitudes [42–44]. These techniques work best if all external particles carry color charges, while their implementation becomes more involved as the number of colorless particles in the process increases. The only process which involves *two* colorless particles and jets in the final state that has been computed with unitarity methods before, $pp \to W^+W^+jj$ [24], is simpler than the calculation presented here since, among other things, only a smaller number of subprocesses contribute. As explained in the next section, the presence of two colorless particles in the final state whose total electric charge is zero provides some additional difficulty. Nevertheless, it is possible to handle these complications with on-shell methods.

The remainder of the paper is organized as follows. In Sec. II, we provide technical details of the calculation. In Sec. III we discuss phenomenological results for the QCD production of W^+W^-jj, with leptonic decays of the W-bosons, at the Tevatron and the LHC. We conclude in Sec. IV. We provide numerical results for various one-loop primitive amplitudes, as well as squared amplitudes summed over helicity and color for $(W^+ \to \nu_\mu \mu^+) + (W^- \to e^- \bar{\nu}_e)jj$ hadronic production in the Appendix.

II. TECHNICAL DETAILS

In this section we present technical details specific to this calculation. Within a subtraction formalism, a NLO calculation involves three components: virtual corrections, real emission corrections, and subtraction terms for soft and collinear divergences. The virtual corrections

are computed using D-dimensional generalized unitarity [8,9]. A detailed description of the implementation of this method can be found in [45]; we have followed this implementation, modifying and extending it to deal with the presence of an additional W-boson in the final state.

The full one-loop amplitude can be built by summing products of color-ordered partial amplitudes [42–44] over all permutations of the colored particles, with appropriate color factors. The partial amplitudes are further decomposed into primitive amplitudes. The ordering of all particles with color charges is fixed in primitive amplitudes. D-dimensional unitarity cuts reduce one-loop primitive amplitudes to linear combinations of products of tree-level helicity amplitudes, which are computed using Berends-Giele recursion relations [46]. These relations are also used to compute tree-level amplitudes which are required for calculations of LO cross-sections, real emission corrections and subtraction terms for soft and collinear emissions. We implement subtraction terms following the Catani-Seymour procedure [47], with the α-parameter optimization as described in Refs. [48,49]. We embed our calculations within the framework of the MCFM program [50] and use the QCDLOOP program to calculate the scalar one-loop integrals [51].

Since only color-charged particles are ordered in primitive amplitudes, all possible insertions of the W-bosons must be considered when tree-level or one-loop primitive amplitudes are computed. While this implies a certain amount of nontrivial bookkeeping in the construction of a numerical program, this can be done without much trouble. The real problem, however, is that cuts of different parent diagrams must be combined in certain cases to produce gauge-invariant tree-level amplitudes in the context of unitarity cuts. This implies that different parent diagrams cannot be treated independently and this creates considerable overhead. Furthermore, we must include the possibility of the W^+W^- pair being produced via an intermediate neutral vector boson, such as an off-shell γ or Z.

In this calculation, we do not consider the production of top quarks in the final state, as these are processes with a distinct experimental signature. Furthermore, we neglect top-quark contributions in virtual diagrams and treat all other quarks as massless. Since top quarks in virtual diagrams originate from $b \to Wt^*$ transitions, we decided to completely exclude bottom quarks in our calculation as well. This is a reasonable approximation since the b-content of the proton is subdominant both at the Tevatron and the LHC. We also neglect $g^* \to b\bar{b}$ splitting, both real and virtual. We believe that this effect is also quite small as can be seen from the b-quark contribution to the QCD β-function, relative to contributions of gluons and four other quarks. Although we do not expect that the complete omission of quarks in the third generation impacts our results in any significant way, we hope to include them in the calculation in the future. The framework to do so, within the generalized D-dimensional unitarity approach, has already been fully elaborated in Refs. [52,53]. Before continuing, we point out that in this paper we do not include contributions from one-loop diagrams where the γ/Z or the W^+W^- pair couple directly to a loop of virtual quarks, creating a diagram of the "light-by-light scattering" type. These diagrams form a finite, gauge-invariant class of amplitudes that can be dealt with separately. In particular, amplitudes for the partonic process $gg \to W^+W^-gg$ which does not appear at tree-level also belong to that class of amplitudes. As pointed out in Ref. [54], processes of that type may be quite important because of the large gluon flux at the LHC. We plan to return to the discussion of the amplitudes where W^+W^- pair couples directly to a closed quark loop in a separate publication. Finally, in this calculation we neglect mixing between up and down quarks of different generations and set the CKM matrix to the identity matrix.

The production of W^+W^-jj can occur through both electroweak and QCD mechanisms. The NLO QCD corrections for the electroweak production have already been calculated in Ref. [55]. While these mechanisms can interfere even at leading order, these interference terms are strongly suppressed. First, at partonic level, the electroweak production of W^+W^-jj involves four quarks. However, given the large gluon luminosity at the LHC, four-quark contributions to the W^+W^-jj production cross section amount to only about 15%. Moreover, the interference that occurs in a four-quark process can only happen for certain combinations of quark flavors, and it is color-suppressed. We therefore neglect this interference, and present results for the QCD production alone.

In order to describe tree-level and one-loop virtual corrections to $pp(p\bar{p}) \to W^+W^-jj$ we require partonic processes with either two quarks and two gluons $0 \to \bar{q}_1 q_2 g g W^+W^-$ or with four quarks $0 \to \bar{q}_1 q_2 \bar{q}_3 q_4 W^+W^-$. Given the difference in color- and flavor structures, we discuss these two partonic processes separately in the next two subsections.

A. Processes with W^+W^- pair, a quark pair and two gluons

In this section, we consider the partonic process $0 \to \bar{q}_1 q_2 g g W^+W^-$. Since we neglect mixing between up and down quarks of different generations, in two-quark amplitudes both quarks $q_{1,2}$ have the same flavor.

To obtain the full NLO cross section, we need to consider all possible crossings between the partons; the initial state partons—as well as the jets—may be either gluons or quarks. The tree-level amplitude for the process $0 \to (\bar{q}q) + (W^+ \to \nu_\mu + \mu^+) + (W^- \to e^- + \bar{\nu}_e) + g + g$ can be written as

$$\mathcal{A}^{\text{tree}}(\bar{q}_1, q_2;, \nu_\mu, \mu^+, e^-, \bar{\nu}_e; g_3, g_4) = g_s^2\left(\frac{g_W}{\sqrt{2}}\right)^4 P_W(s_{\nu_\mu\mu^+})P_W(s_{e^-\bar{\nu}_e})((T^{a_3}T^{a_4})_{\bar{i}_1 i_2} \times A_0(\bar{q}_1, q_2; g_3, g_4) + (T^{a_4}T^{a_3})_{\bar{i}_1 i_2}A_0(\bar{q}_1, q_2; g_4, g_3)). \tag{2.1}$$

In Eq. (2.1), g_s and g_W are the strong and weak coupling constants, respectively, leptonic labels have been suppressed on the right-hand side, and P_W are Breit-Wigner propagators

$$P_W(s) = \frac{s}{s - M_W^2 + i\Gamma_W M_W}, \tag{2.2}$$

with $s_{l\nu} = (p_l + p_\nu)^2$. In addition, M_W and Γ_W are the W-boson mass and width, and the generators of the $SU(3)$ color group are normalized to $\text{Tr}(T^a T^b) = \delta^{ab}$. In Eq. (2.1), A_0 denote the color-ordered amplitudes. The flavor of the quark line fixes the electric charges of q_1 and q_2 and, simultaneously, the ordering of W^+ and W^- along the quark line. However, as we pointed out before, the relative ordering of $W^\pm$ bosons and gluons is not fixed. Additionally, we need to consider the possibility that W-bosons are produced through an intermediate (off-shell) Z-boson or photon. Thus we write

$$A_0(\bar{q}_1, q_2; g_3, g_4) = A_0^{(WW)}([\bar{q}_1, W, W, q_2]; g_3, g_4) + C^{(q_2,h_2)}A_0^{(\gamma/Z)}([\bar{q}_1, \gamma/Z, q_2]; g_3, g_4), \tag{2.3}$$

where the first term describes an amplitude where W-bosons couple directly to the quark line and the second term describes an amplitude where such coupling occurs through a γ or Z. The factor $C^{(q_2,h_2)}$ is given by

$$C^{(q,h)} = 2Q^{(q)}\sin^2\theta_W + P_Z(s_Z)(T_3^{(h)} - 2Q^{(q)}\sin^2\theta_W), \tag{2.4}$$

where $Q^{(q)}$ and h are the electromagnetic charge and helicity of the quark q, $T_3^{(-)} = 1$ and $T_3^{(+)} = 0$, θ_W is the weak mixing angle, and $s_Z = (p_{W^+} + p_{W^-})^2 = (p_{\nu_\mu} + p_{\mu^+} + p_{e^-} + p_{\bar{\nu}_e})^2$. Note that, because W-bosons only couple to left-handed quarks, the first term in Eq. (2.3) is zero if the quark is right-handed. We account for the decay $W^\pm \to l^\pm(p_l) + \nu_l(p_\nu)$, by using the $W^\pm$ polarization vectors constructed from lepton spinors. For example, in case of the W^+ boson, the polarization vector reads

$$\epsilon_-^\mu(p_\nu, p_{l^+}) = \frac{\bar{u}(p_\nu)\gamma^\mu\gamma_- v(p_{l^+})}{(p_{l^+} + p_\nu)^2}; \qquad \gamma_- = \frac{1 - \gamma_5}{2}. \tag{2.5}$$

The computation of real emission contributions requires tree amplitudes with an additional gluon in the final state. The color decomposition reads

$$\mathcal{A}^{\text{tree}}(\bar{q}_1, q_2; \nu_\mu, \mu^+, e^-, \bar{\nu}_e; g_3, g_4, g_5) = g_s^3\left(\frac{g_W}{\sqrt{2}}\right)^4 P_W(s_{\nu_\mu\mu^+})P_W(s_{e^-\bar{\nu}_e})\sum_{\sigma\in S_3}(T^{a_{\sigma_3}}T^{a_{\sigma_4}}T^{a_{\sigma_5}})_{\bar{i}_1 i_2} \times A_0(\bar{q}_1, q_2; g_{\sigma_3}, g_{\sigma_4}, g_{\sigma_5}), \tag{2.6}$$

where S_i denotes the permutation of i indices. The flavor/helicity properties of the amplitudes with three and two gluons are identical and have been discussed for the two-gluon case.

The decomposition of the one-loop amplitudes in terms of left-handed primitive amplitudes [42,45] reads

$$\mathcal{A}^{1\text{L}}(\bar{q}_1, q_2; \nu_\mu, \mu^+, e^-, \bar{\nu}_e; g_3, g_4) = g_s^4\left(\frac{g_W}{\sqrt{2}}\right)^4 P_W(s_{\nu_\mu\mu^+})P_W(s_{e^-\bar{\nu}_e})\sum_{\sigma\in S_2}[(T^{x_2}T^{a_{\sigma_3}}T^{a_{\sigma_4}}T^{x_2})_{\bar{i}_1 i_2} \times A_1(\bar{q}_1, g_{\sigma_4}, g_{\sigma_3}, q_2) + (T^{x_2}T^{a_{\sigma_3}}T^{x_1})_{\bar{i}_1 i_2}(f^{a_{\sigma_4}})_{x_1 x_2} \times A_1(\bar{q}_1, g_{\sigma_3}, q_2, g_{\sigma_4}) + (T^{x_2}T^{x_1})_{\bar{i}_1 i_2}(f^{a_{\sigma_3}}f^{a_{\sigma_4}})_{x_1 x_2} \times A_1(\bar{q}_1, q_2, g_{\sigma_4}, g_{\sigma_3}) + \frac{n_f}{N_c}\text{Gr}_4 A_1^{[1/2]}(\bar{q}_1, q_2, g_{\sigma_3}, g_{\sigma_4})]. \tag{2.7}$$

In Eq. (2.7) we introduced the color factor

$$\text{Gr}_4 = N_c(T^{a_{\sigma_3}}T^{a_{\sigma_4}})_{\bar{i}_1 i_2} - \text{Tr}(T^{a_{\sigma_3}}T^{a_{\sigma_4}})\delta_{\bar{i}_1 i_2}. \tag{2.8}$$

We build up the virtual amplitude from eight primitive amplitudes: $A_1(\bar{q}_1, g_4, g_3, q_2)$, $A_1(\bar{q}_1, g_3, q_2, g_4)$, $A_1(\bar{q}_1, q_2, g_4, g_3)$ and $A_1^{[1/2]}(\bar{q}_1, q_2, g_3, g_4)$, shown in Fig. 1 and

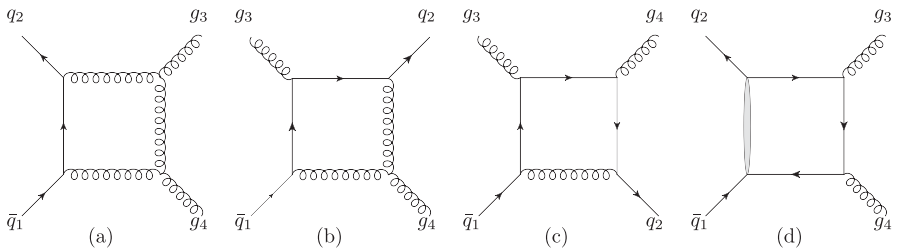

FIG. 1. Primitive amplitudes (a) $A_1(\bar{q}_1, q_2, g_3, g_4)$, (b) $A_1(\bar{q}_1, g_3, q_2, g_4)$, (c) $A_1(\bar{q}_1, g_3, g_4, q_2)$, and (d) $A_1^{[1/2]}(\bar{q}_1, q_2, g_3, g_4)$. W bosons are not shown.

another four amplitudes, obtained by swapping the gluons $g_3 \leftrightarrow g_4$. In Fig. 1, we introduce a "dummy line" for the primitive amplitude $A_1^{[1/2]}(\bar{q}_1, q_2, g_3, g_4)$. This allows us to draw this primitive amplitude—which has the external gluons attached to a fermion loop—as formally having six loop-momentum-dependent propagators.[1] The W-bosons couple to the dummy lines, but dummy lines cannot be cut.

B. Processes with W^+W^- and two quark pairs

We now consider the case of amplitudes involving two $\bar{q}q$ pairs and the W^+W^- pair. We first discuss the color and flavor structure of the tree-level amplitude $0 \to (\bar{q}_1 q_2 \bar{q}_3 q_4) + (W^+ \to \nu_\mu + \mu^+) + (W^- \to e^- + \bar{\nu}_e)$ treating all particles as being in the final state. This process is described by Feynman diagrams with two continuous fermion lines connected by a gluon exchange, with W-bosons being emitted from either of the two quark lines. Depending on the quark flavors *and* on the way the W-boson emissions occur, we may have to assign quark fields in two different ways to the fermion lines: $[\bar{q}_1 q_2]$, $[\bar{q}_3 q_4]$ and $[\bar{q}_1 q_4]$, $[\bar{q}_3 q_2]$. We refer to the first assignment as the "s-channel amplitude" and to the second assignment as the "t-channel amplitude", see Fig. 2.

We begin by considering the s-channel tree-level amplitude. In this case, the color decomposition reads

$$\begin{aligned}\mathcal{B}^{\text{tree}}&(\bar{q}_1, q_2; \bar{q}_3, q_4; \nu_\mu, \mu^+, e^-, \bar{\nu}_e) \\ &= g_s^2 \left(\frac{g_W}{\sqrt{2}}\right)^4 P_W(s_{e^+\nu_e}) P_W(s_{\mu^-\nu_\mu}) \\ &\quad \times \left(\delta_{\bar{i}_1 i_4}\delta_{\bar{i}_3 i_2} - \frac{1}{N_c}\delta_{\bar{i}_1 i_2}\delta_{\bar{i}_3 i_4}\right) B_0(\bar{q}_1, q_2; \bar{q}_3, q_4). \quad (2.9)\end{aligned}$$

We can further split the B_0 amplitude into two separate types. The amplitude of the first type appears if a quark line radiates both W-bosons and the other quark line radiates none. The W-boson can be radiated either directly from the quark line, or through an exchange of an intermediate γ/Z. The amplitude of the second type arises when one W-boson is radiated from each of the quark lines. Examples of the corresponding contributions are shown in Figs. 3 and 4 for specific flavor assignments; it is clear how this classification generalizes to other flavors.

We begin by discussing amplitudes of the first type. Since we set the CKM matrix equal to the identity matrix, flavors of fermions can not change along the fermion lines, so that flavors of $\bar{q}_1$ and q_2 as well as of $\bar{q}_3$ and q_4 are equal. Thus, for a set of flavor assignments, for which this contribution is allowed, there are four diagrams that contribute to the amplitude B_0. Examples are shown in Fig. 3. We write the color-ordered amplitude as

[1]We count external W-bosons, which are not shown in Fig. 1.

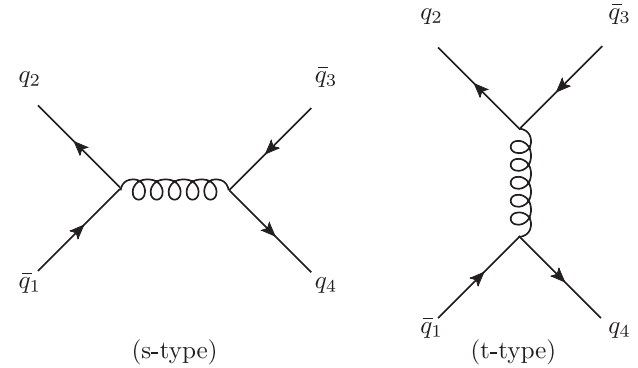

FIG. 2. Amplitudes of s-type (left) and of t-type (right), for the partonic process $0 \to W^+W^-\bar{q}_1 q_2 \bar{q}_3 q_4$. The W-bosons are not shown.

$$\begin{aligned}B_0(\bar{q}_1, q_2; \bar{q}_3, q_4) &= B_0^{(WW)}([\bar{q}_1, W, W, q_2], [\bar{q}_3, q_4]) \\ &\quad + B_0^{(WW)}([\bar{q}_1, q_2], [\bar{q}_3, W, W, q_4]) \\ &\quad + C^{(q_2,h_2)} B_0^{(\gamma/Z)}([\bar{q}_1, \gamma/Z, q_2], [\bar{q}_3, q_4]) \\ &\quad + C^{(q_4,h_4)} B_0^{(\gamma/Z)}([\bar{q}_1, q_2], [\bar{q}_3, \gamma/Z, q_4]), \quad (2.10)\end{aligned}$$

where $h_{2,4} = \{-, +\}$ are the helicities of quarks q_2 and q_4. We note that since W-bosons couple only to left-handed quarks, the first term in Eq. (2.10) is zero for $h_2 = 1$, and the second term is zero for $h_4 = 1$. The factors $C^{(q,h)}$ are given in Eq. (2.4). The second term in Eq. (2.10) can be obtained from the first term by swapping momenta $p_{\bar{q}_1} \leftrightarrow p_{\bar{q}_3}$ and $p_{q_2} \leftrightarrow p_{q_4}$. The same swap can be used to obtain the fourth term in Eq. (2.10) from the third.

We turn to the discussion of the amplitudes of the second type, which correspond to the emission of the W^+ boson off one quark line and the W^- boson off the other quark line. As a result of the emission, flavors change along each

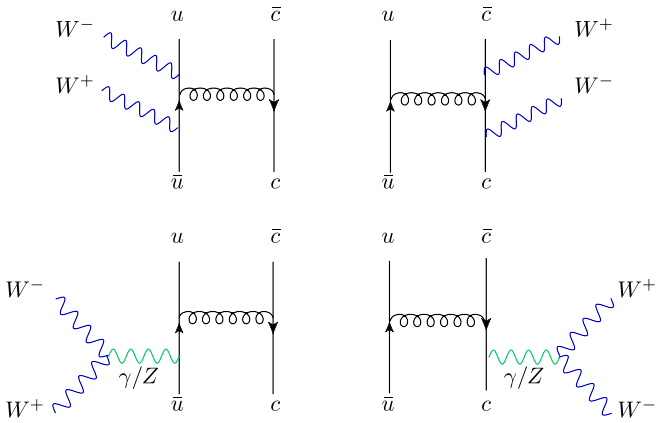

FIG. 3 (color online). Sample tree-level diagrams for $B_0(\bar{u}, u, \bar{c}, c)$. When both W-bosons couple directly to the quark line, the flavors of the quarks determine the ordering of the W-bosons.

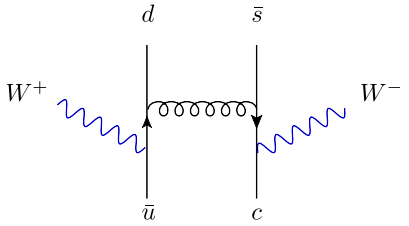

FIG. 4 (color online). Sample tree-level diagram for $B_0(\bar{u}, d, \bar{s}, c)$.

fermion line. An example of a diagram contributing to this amplitude is shown in Fig. 4. As there is no contribution of the neutral vector boson in this case, the amplitude is nonzero only for $h_2 = h_4 = -1$. The choice of flavors for $\bar{q}_1$, $\bar{q}_3$ determine which W-boson is radiated from which quark line.

According to the flavors of the four quarks, only one of the s- or t-channel amplitudes can contribute, or both. Since the t-channel amplitude is obtained by replacing $q_2 \leftrightarrow q_4$ in the s-channel amplitude, everything that has been said about the latter applies to the former. Note that the replacement $q_2 \leftrightarrow q_4$ also involves color indices, so that nontrivial color-correlations appear in the interference of s- and t-channel amplitudes when both are allowed by flavor.

For the computation of real emission corrections we need four-quark amplitudes with additional gluon in the final state $0 \to (\bar{q}_1 q_2 \bar{q}_3 q_4) + (W^+ \to \nu_\mu + \mu^+) + (W^- \to e^- + \bar{\nu}_e) + g$. It is clear that the presence of an additional gluon does not modify the separation of amplitudes into s- and t-channel amplitudes, so that much of what has been said about the tree-level amplitudes remains applicable. In particular, the flavor structure is identical to the tree-level case discussed above. On the other hand, the color decomposition differs. For instance, for the s-channel amplitude, it reads

$$\begin{aligned}\mathcal{B}^{\text{tree}}(\bar{q}_1, q_2, \bar{q}_3, q_4, g; \nu_\mu, \mu^+, e^-, \bar{\nu}_e) = g_s^3\left(\frac{g_W}{\sqrt{2}}\right)^4 P_W(s_{\nu_\mu \mu^+}) P_W(s_{e^- \bar{\nu}_e}) \Big[& \delta_{\bar{i}_3 i_2} T^a_{\bar{i}_1 i_4} B_0(\bar{q}_1, q_2, \bar{q}_3, q_4, g) \\ & + \frac{1}{N_c} \delta_{\bar{i}_3 i_4} T^a_{\bar{i}_1 i_2} B_0(\bar{q}_1, g, q_2, \bar{q}_3, q_4) + \delta_{\bar{i}_1 i_4} T^a_{\bar{i}+3 i_2} B_0(\bar{q}_1, q_2, g, \bar{q}_3, q_4) \\ & + \frac{1}{N_c} \delta_{\bar{i}_1 i_2} T^a_{\bar{i}_3 i_4} B_0(\bar{q}_1, q_2, \bar{q}_3, g, q_4) \Big]. \end{aligned} \tag{2.11}$$

Similar considerations apply to virtual corrections but the color decomposition is more involved in this case. For the s-channel virtual QCD amplitude it reads

$$\begin{aligned}\mathcal{B}^{\text{1L}}(\bar{q}_1, q_2, \bar{q}_3, q_4; \nu_\mu, \mu^+, e^-, \bar{\nu}_e) = g_s^4\left(\frac{g_W}{\sqrt{2}}\right)^4 P_W(s_{\nu_\mu, \mu^+}) P_W(s_{e^- \bar{\nu}_e}) (\delta_{\bar{i}_1 i_4} \delta_{\bar{i}_3 i_2} B_1^{(1)}(\bar{q}_1, q_2, \bar{q}_3, q_4) \\ + \delta_{\bar{i}_1 i_2} \delta_{\bar{i}_3 i_4} B_1^{(2)}(\bar{q}_1, q_2, \bar{q}_3, q_4)). \end{aligned} \tag{2.12}$$

The amplitudes in Eq. (2.12) are written through primitive amplitudes as

$$\begin{aligned} B_1^{(1)}(\bar{q}_1, q_2, \bar{q}_3, q_4) = & \left(N_c - \frac{2}{N_c}\right) B_1^{(a)}(\bar{q}_1, q_2, \bar{q}_3, q_4) - \frac{2}{N_c} B_1^{(a)}(\bar{q}_1, q_2, \bar{q}_3, q_4) - \frac{1}{N_c} B_1^{(b)}(\bar{q}_1, q_2, \bar{q}_3, q_4) \\ & - \frac{1}{N_c} B_1^{(c)}(\bar{q}_1, q_2, \bar{q}_3, q_4) + n_f B_1^{(d)}(\bar{q}_1, q_2, \bar{q}_3, q_4), \end{aligned} \tag{2.13}$$

and

$$\begin{aligned} B_1^{(2)}(\bar{q}_1, q_2, \bar{q}_3, q_4) = & \frac{1}{N_c^2} B_1^{(a)}(\bar{q}_1, q_2, \bar{q}_3, q_4) + \left(1 + \frac{1}{N_c^2}\right) B_1^{(a)}(\bar{q}_1, q_2, \bar{q}_3, q_4) + \frac{1}{N_c^2} B_1^{(b)}(\bar{q}_1, q_2, \bar{q}_3, q_4) \\ & + \frac{1}{N_c^2} B_1^{(c)}(\bar{q}_1, q_2, \bar{q}_3, q_4) - \frac{n_f}{N_c} B_1^{(d)}(\bar{q}_1, q_2, \bar{q}_3, q_4). \end{aligned} \tag{2.14}$$

Parent diagrams for the primitive amplitudes $B_1^{(a,b,c,d)}$ are shown in Fig. 5. The only primitive amplitude that receives contributions from six-point one-loop diagrams is $B^{(a)}$. Primitives $B^{(b)}$ and $B^{(c)}$ are simply the Born amplitudes dressed by a gluon loop on one of the quark lines, while $B^{(d)}$ corresponds to a fermion loop contribution. For convenience, we again use dummy lines in Fig. 5; they allow us to consider every primitive amplitude as having a parent diagram with (formally) six propagators. We recall that W-bosons couple to dummy lines, but that these lines

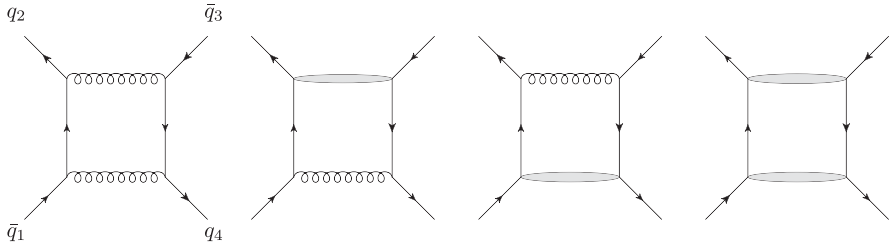

FIG. 5. Parent diagrams for one-loop primitive amplitudes $B_1^{(a,b,c,d)}$ for $0 \to (\bar{q}_1 q_2 \bar{q}_3 q_4) + W^+W^-$, where the flavors of the quarks are not specified. The W-bosons are not shown. Shaded areas represent dummy lines which are not cut.

cannot be cut. Berends-Giele recursion relations are modified in these cases to ensure that the correct primitive amplitudes are recovered.

C. Checks on the calculation

Various checks were carried out at all stages of the calculation. The squared matrix elements for the leading order and real emission processes were checked against MADGRAPH [56] for a few phase space points. This was done for all flavor combinations and all initial state parton configurations. Gauge invariance of various amplitudes was checked for both the external gluons and the W-bosons (artificially setting the masses of the latter to zero), at leading and next-to-leading order. The subtraction terms of the Catani-Seymour dipole method were checked to cancel with the real emission terms in the limit when emitted partons become soft and/or collinear. We checked the double and single infrared poles of the virtual contribution, both at the level of primitive amplitudes and at the level of virtual matrix elements squared. These terms were also checked to cancel with the integrated dipoles. We also checked the independence of the cross section of the α-parameter [48,49]. Finally, the full one-loop amplitude is checked against an OPP-based, but otherwise completely independent diagrammatic computation, at a few phase space points. We note that over 600 Feynman diagrams are involved in a such a calculation.

By default, our calculation was performed in double precision. For each phase space point, the double and single poles were checked against the analytically known results, and the coefficients of the OPP expansion were checked to have accurately solved the system of linear equations. If either of those checks failed, the amplitude at that phase space point was recalculated using quadruple precision. We found that around 0.4% of primitive amplitudes had to be recalculated this way.

III. PHENOMENOLOGY

In this section, we discuss phenomenological aspects of W^+W^-jj production at the Tevatron and the LHC. At the Tevatron, this process is a background to Higgs-boson production in association with two jets. We employ set of cuts discussed in the context of the Higgs-boson search in Ref. [29] and study related phenomenology. At the LHC, we consider the collision energy of 7 TeV and we show that the number of dilepton events related to W^+W^-jj production is sufficiently large to study this process in detail.

Before moving on to a dedicated discussion, we briefly describe general features of our computation. The W-bosons are always produced on mass-shell and decay leptonically $W^+W^- \to \nu_\mu \mu^+ e^- \bar{\nu}_e$. We note that, neglecting nonresonant contributions, the results for all lepton flavors $l^+l^- = \{e^+e^-, e^+\mu^-, \mu^+e^-, \mu^+\mu^-\}$ can be obtained by multiplying our results by four.

The mass and width of the W-boson are taken to be $M_W = 80.419$ GeV and $\Gamma_W = 2.141$ GeV, respectively. The width of the Z-boson is taken to be $\Gamma_Z = 2.49$ GeV. The propagators for these particles take the Breit-Wigner form. The electroweak gauge couplings are computed using $\alpha_{\rm QED}(M_Z) = 1/128.802$ and $\sin^2\theta_W = 0.2222$. We use MSTW08LO parton distribution functions for leading-order and MSTW08NLO for next-to-leading-order computations [57]. The strong coupling constant $\alpha_s(M_Z)$ is part of the MSTW fit. It equals to 0.13939 (0.12018) at leading- and next-to-leading order, respectively.

A. Results for the Tevatron

By the end of Run II, the Tevatron will have collected just over 10 fb^{-1} of data for use in the search for the Higgs boson. At the very least, the two Tevatron experiments will be able to improve upon the exclusion limits for the Higgs bosons presented earlier in Ref. [58]. The search strategy is to separate relevant processes, depending on the number of jets produced with the Higgs boson. As follows from the analysis in Ref. [59], 10% of all events with the Higgs boson at the Tevatron contain two or more jets. The process $pp \to W^+W^-jj$ is a SM background of significant importance. In Ref. [59], the NLO QCD cross section for Higgs $+2$ jet production with the decay $H \to W^-(\to \mu^-\bar{\nu}_\mu)W^+(\to \nu_e e^+)$ is calculated. For the Higgs-boson mass of 160 GeV, the cross-section value $\sigma_{\rm NLO} = 0.2$ fb is found (we do not show the uncertainties which are significant). This cross section is obtained with cuts that are similar to those used by the CDF Collaboration in their Higgs-boson search [29]. Specifically, jets are defined using the $k_\perp$-algorithm, with $\Delta R_{j_1 j_2} > 0.4$. Jets must have

$p_{\perp,j} > 15$ GeV and must be in the central region of the detector, $|\eta_j| < 2.5$. It is required that two leptons, one with transverse momentum $p_{\perp,l_1} > 20$ GeV and rapidity $|\eta_{l_1}| < 0.8$ and the other with transverse momentum $p_{\perp,l_2} > 10$ GeV and rapidity $|\eta_{l_2}| < 1.1$, appear in the event. The invariant mass of the lepton pair is required to be larger than $m_{l_1 l_2} > 16$ GeV. Both leptons must be isolated. The specific requirement to this effect is that any jet within $\Delta R = 0.4$ of a lepton must have a transverse momentum which is smaller than $0.1 p_{\perp,l}$. The CDF Collaboration uses a particular constraint on the missing transverse momentum. They introduce a function

$$E_{\perp}^{\text{spec}} = E_{\perp} \sin\left[\min\left(\Delta\phi, \frac{\pi}{2}\right)\right],$$

with $\Delta\phi$ being the angle between the missing transverse momentum vector $E_{\perp}$ and the nearest lepton or jet. An event is accepted if $E_{\perp}^{\text{spec}} > 25$ GeV.

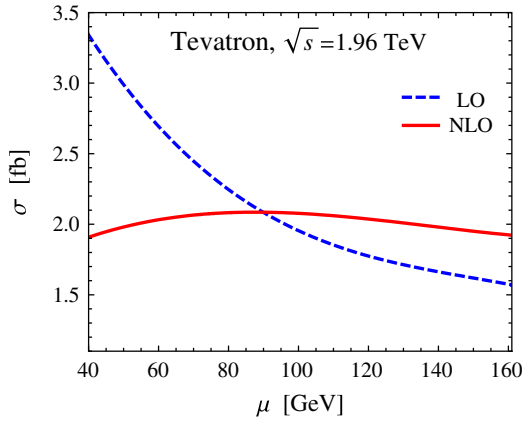

FIG. 6 (color online). The dependence on renormalization and factorization scale of the cross section for $p\bar{p} \to \nu_\mu \mu^+ e^- \bar{\nu}_e jj$ at $\sqrt{s} = 1.96$ TeV, where $\mu = \mu_R = \mu_F$. Predictions at both LO and NLO in QCD are shown.

We present NLO QCD results for the process $p\bar{p} \to W^+(\to \nu_\mu \mu^+) W^-(\to e^- \bar{\nu}_e) jj$, at $\sqrt{s} = 1.96$ TeV, using the kinematic cuts that we just described. This allows us to study this process as a background to the Higgs-boson production. In Fig. 6 we show the scale dependence of the cross section for the process $p\bar{p} \to W^+(\to \nu_\mu \mu^+) W^-(\to e^- \bar{\nu}_e) jj$, both at LO and NLO in perturbative QCD (pQCD), with the scale ranging between $M_W/2$ and $2M_W$.

The leading-order cross section is $\sigma_{\text{LO}} = 2.5 \pm 0.9$ fb. This result is interesting since *its uncertainty alone exceeds the cross section for the production of the Higgs boson in association with two jets by about a factor between four and five*. Clearly, there is no way to discuss observation of the Higgs boson in this channel unless the theoretical uncertainty on $W^+W^- jj$ is improved. The situation indeed improves once NLO QCD corrections are computed. We find $\sigma_{\text{NLO}} = 2.0 \pm 0.1$ fb—a significant reduction in scale uncertainty. However, even after that reduction, we find that the *uncertainty* on the $W^+W^- jj$ production cross section is very much comparable to the *absolute value* of the Higgs-boson production cross section in association with two jets. For this set of cuts, the NLO QCD computations lead to a prediction of about 80 $e\mu^+ jj$, $e^+\mu jj$, $e^+e^- jj$, $\mu^+\mu^- jj$ events during Run II, using the discussed set of cuts and assuming 100% efficiency.

There are other kinematic variables that one can use to improve upon a discrimination between the Higgs-boson production and the W^+W^- production. For example, the opening angle of the two leptons is of particular interest. Indeed, if a pair of W-bosons is produced in the decay of a scalar particle, their spins are anticorrelated. As a result, leptons from their decay tend to have small relative angles

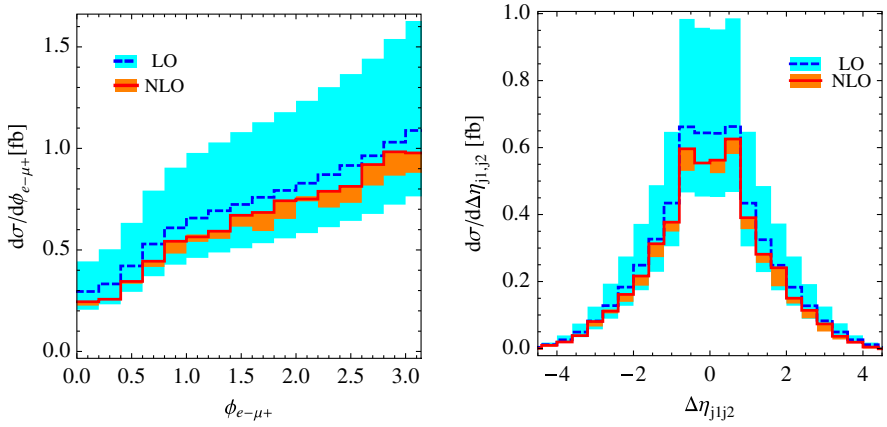

FIG. 7 (color online). Kinematic distributions showing the opening angle between the leptons, $\phi_{e^-\mu^+}$, and the difference in rapidity of the two hardest jets, for the process $p\bar{p} \to W^+(\to \nu_\mu \mu^+) W^-(\to e^- \bar{\nu}_e) jj$ at the Tevatron running at $\sqrt{s} = 1.96$ TeV. The bands show renormalization and factorization scale uncertainty for $M_W/2 < \mu < 2M_W$, and the solid line is the prediction for $\mu = M_W$.

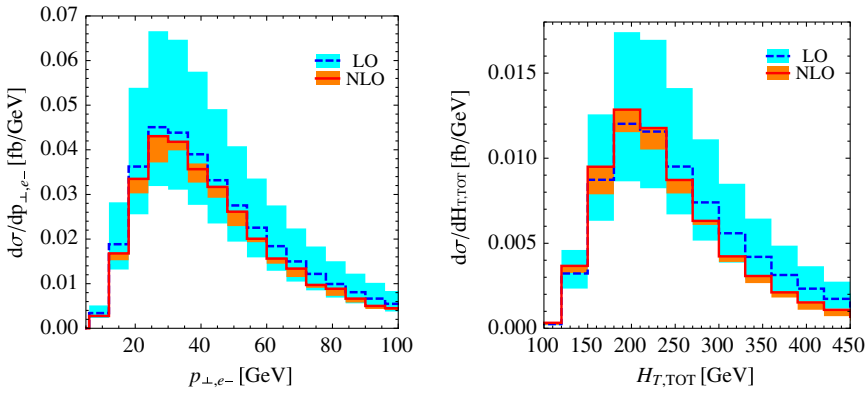

FIG. 8 (color online). Kinematic distributions showing the transverse momentum of a lepton and $H_{T,\mathrm{TOT}}$, for the process $p\bar{p} \to W^+(\to \nu_\mu \mu^+)W^-(\to e^- \bar{\nu}_e)jj$ at the Tevatron running at $\sqrt{s} = 1.96$ TeV. The bands show renormalization and factorization scale uncertainty for $M_W/2 < \mu < 2M_W$, and the solid line is the prediction for $\mu = M_W$.

in the transverse plane. The $\phi_{e^-\mu^+}$ distribution in the case of QCD W^+W^-jj production is shown in Fig. 7 and the leptons are seen to have a preference to be back-to-back, in strong contrast to the Higgs-boson signal. No noticeable shape changes occur when the QCD corrections are included. In the second pane of Fig. 7, we plot the rapidity difference between the two hardest jets $\Delta\eta_{j_1 j_2} = \eta_{j_1} - \eta_{j_2}$, which is peaked at zero and falls off rapidly, with an almost vanishing fraction of the cross section having a magnitude of rapidity difference greater than four. Note that a requirement $|\Delta\eta_{j_1,j_2}| > 4$ is imposed when the Higgs boson is searched for in weak boson fusion.

Finally, Fig. 8 shows the transverse momentum distribution of the charged lepton and $H_{T,\mathrm{TOT}}$ defined as the scalar sum of the transverse momenta of all visible particles present in the final state plus the missing transverse momentum, $H_{T,\mathrm{TOT}} = \sum_j p_{\perp,j} + p_{\perp,\mu^+} + p_{\perp,e^-} + p_{\perp,\mathrm{miss}}$. It follows from Fig. 8 that the shape of lepton transverse momentum distribution does not change but the $H_{T,\mathrm{TOT}}$ distribution becomes somewhat softer at NLO QCD.

B. Results for the LHC

The LHC is set to run at 7 TeV until the end of 2012, collecting 2–5 fb^{-1} of data. As a result, a non-negligible number of dilepton events, originating from W^+W^-jj, will be observed at the LHC during this and next year, which warrants a phenomenological study of this process. The importance of $pp \to W^+W^-jj$ process as a background to Higgs-boson production has been discussed extensively in the literature (see e.g. [60]), especially with reference to the weak boson fusion production mechanism, where designed cuts on the jets can dramatically boost the signal to background ratio. In this paper, we do not employ the weak boson fusion cuts, opting instead for a selection criteria that give sizable cross sections for $pp \to W^+W^-jj$. Our choice of cuts is inspired by those that are made in the first analyses of $t\bar{t}$ production by ATLAS and CMS Collaborations [61,62]. We do, however, plot distributions which are interesting in the context of reducing the W^+W^-jj background to the Higgs-boson searches in weak boson fusion. For example, we study the relative jet rapidity $\Delta\eta_{j_1 j_2} = \eta_{j_1} - \eta_{j_2}$ distribution and the opening azimuthal angle of the two leptons $\phi_{l_1 l_2}$. Given that the center-of-mass energy of collisions at the LHC after the longer shutdown at the end of 2012 is not fully decided yet, we also find it interesting to show the behavior of the cross section as a function of $\sqrt{s}$.

We consider proton-proton scattering $pp \to W^+W^-jj$ at center-of-mass energy $\sqrt{s} = 7$ TeV. We impose the following cuts, inspired by $t\bar{t}$ searches at the LHC:

(i) jets are defined using the anti-$k_\perp$ algorithm [63] as implemented in FastJet [64], with

$$\Delta R_{j_1 j_2} = \sqrt{(\eta_{j1} - \eta_{j2})^2 + (\phi_{j1} - \phi_{j2})^2} > 0.4; \tag{3.1}$$

(ii) jets are required to have transverse momentum $p_{\perp,j} > 30$ GeV and the rapidity $|\eta_j| < 3.2$;

(iii) charged leptons are required to have transverse momenta $p_{\perp,l} > 20$ GeV and the rapidity $|\eta_l| < 2.4$;

(iv) missing transverse momentum is required to satisfy $p_{\perp,\mathrm{miss}} > 30$ GeV.

In the left pane of Fig. 9 we show the dependence of the cross section $pp \to W^+W^- \to \mu^+\nu_\mu e\bar{\nu}_e jj$ at the 7 TeV run of the LHC, on the factorization and renormalization scales, which we set equal to each other. At leading-order, the cross-section falls with the scale μ, which is attributable to the behavior of the strong coupling α_s. Considering a range of factorization/renormalization scales $M_W < \mu < 4M_W$ and choosing the central value $\mu = 2M_W$, we obtain a cross section $\sigma_{\mathrm{LO}} = 46 \pm 13$ fb. At next-to-leading

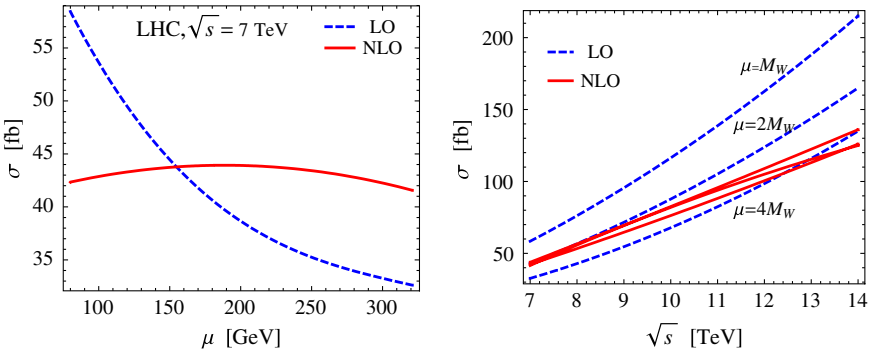

FIG. 9 (color online). In the left pane, we show the production cross section of the process $pp \to (W^+ \to \nu_\mu \mu^+)(W^- \to e^- \bar{\nu}_e) jj$ at the 7 TeV run of the LHC in dependence of the factorization and renormalization scales $\mu_F = \mu_R = \mu$, at LO and NLO in perturbative QCD. In the right pane, the dependence of the cross section on the center-of-mass energy $\sqrt{s}$ is shown. LO results are shown in dashed blue; NLO results are in solid red. Three choices of μ are shown: $\mu = M_W, 2M_W, 4M_W$.

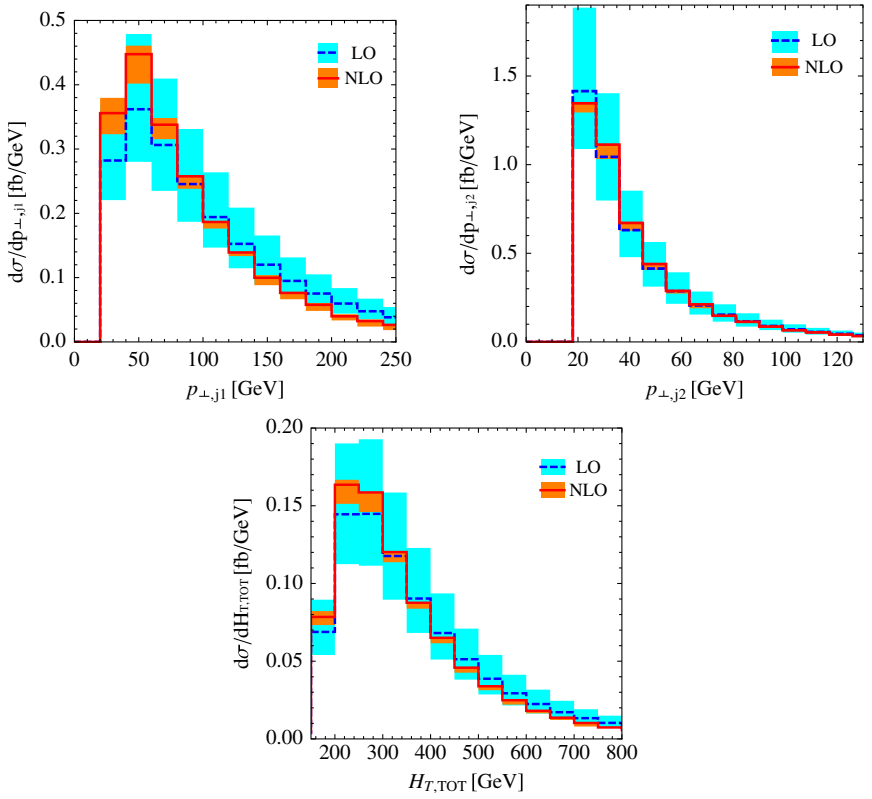

FIG. 10 (color online). Kinematic distributions for jets in the process $pp \to \nu_\mu \mu^+ e^- \bar{\nu}_e jj$ at the 7 TeV run of the LHC at LO and NLO in perturbative QCD. The bands show uncertainty on the renormalization and factorization scale μ, for $M_W \leq \mu \leq 4M_W$, while the lines show results for $\mu = 2M_W$.

order, the dependence on μ is dramatically reduced and the cross section becomes $\sigma_{\rm NLO} = 42 \pm 1$ fb. Such a decrease in the scale dependence is typical of NLO results, and indeed one of the primary motivations for performing calculations at next-to-leading order in pQCD. At the scale $\mu = 2M_W$, the NLO corrections increase the cross section by about 2%. Assuming 50% efficiency, with 5 fb^{-1} of data at the 7 TeV run of the LHC, we expect about 400 dilepton events $e^+\mu^-$, $e\mu^+$, e^+e^-, $\mu^+\mu^-$.

It is interesting to know how the cross section for W^+W^-jj production changes with the collision energy. In the right pane of Fig. 9, we show that the dependence of the NLO cross section on the center-of-mass energy $\sqrt{s}$ is very close to linear. Again, the significant reduction in

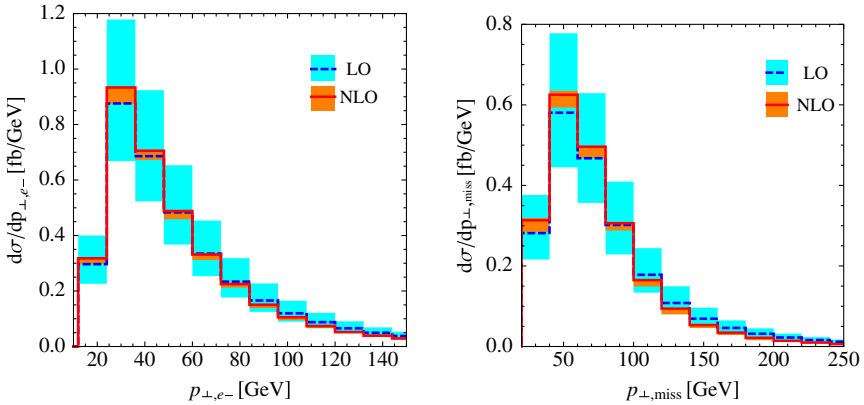

FIG. 11 (color online). Kinematic distributions for leptons in the process $pp \to \nu_\mu \mu^+ e^- \bar{\nu}_e jj$ at the 7 TeV run of the LHC at LO and NLO in perturbative QCD. The bands show uncertainty on the renormalization and factorization scale μ, for $M_W \leq \mu \leq 4M_W$, while the lines show results for $\mu = 2M_W$.

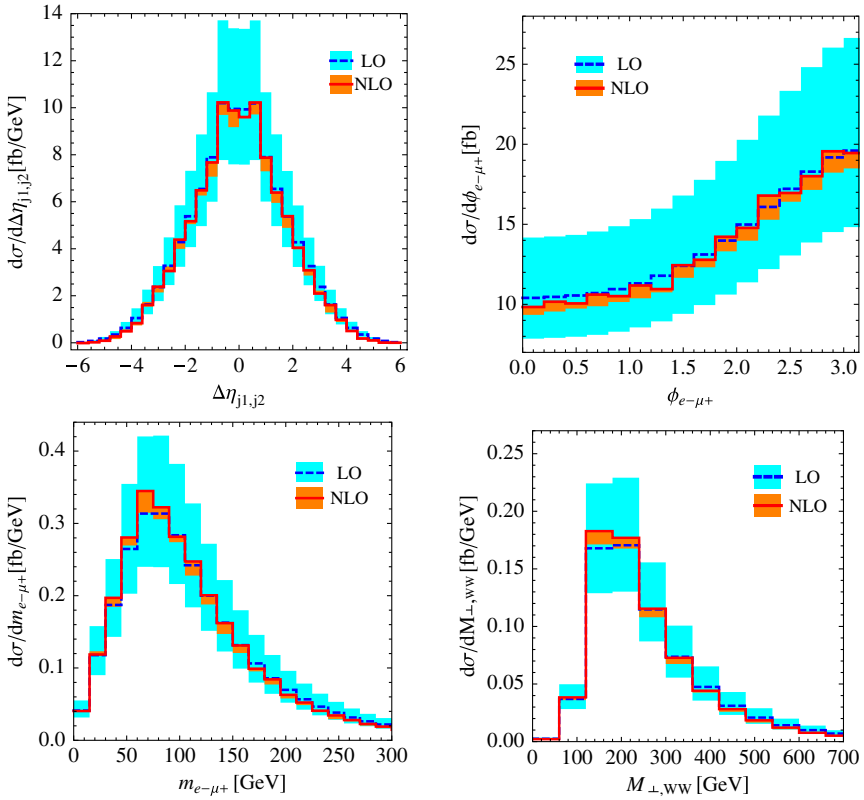

FIG. 12 (color online). Distributions of jet pseudorapidity difference, lepton opening angle and invariant masses for $pp \to \nu_\mu \mu^+ e^- \bar{\nu}_e jj$ at the 7 TeV run of the LHC. LO results are shown in blue; NLO results are in red and orange. The uncertainty bands are for scale $M_W \leq \mu \leq 4M_W$, and the solid lines show the results at $\mu = 2M_W$.

uncertainty in the NLO prediction for the cross section is obvious from Fig. 9. It follows from Fig. 9 that the optimal[2] renormalization/factorization scale increases with the center-of-mass energy smoothly interpolating between $\mu = 2M_W$ at 7 TeV and $\mu = 4M_W$ at 14 TeV.

We now turn to the discussion of kinematic distributions. In Fig. 10 we show the transverse momentum distribution of the hardest and next-to-hardest jets and the distribution of the total transverse energy $H_{T,\mathrm{TOT}}$. For all distributions, the scale dependencies are reduced and shapes of the

[2]We define the "optimal" renormalization/factorization scale as the value of μ for which next-to-leading-order corrections are the smallest.

distributions are, typically, not distorted. Note, however, that the NLO QCD corrections make the jet transverse momenta distributions and the $H_{T,\mathrm{TOT}}$ distributions somewhat softer, which is caused, at least partially, by our use of a constant, rather than a dynamic, renormalization scale in the LO calculation. We show lepton kinematic distributions in Fig. 11. Similar to jet distributions, lepton transverse momentum and the missing energy distributions are softened by the NLO QCD corrections.

A few other distributions which are relevant for designing cuts for Higgs searches are presented in Fig. 12. The distribution of the relative azimuthal angle between the two leptons is peaked at $\phi_{e^-\mu^+} = \pi$, with the NLO corrections making almost no change in the shape of that distribution. The pseudorapidity difference between two leading jets, defined as $\Delta\eta_{j1,j2} = \eta_{j1} - \eta_{j2}$, peaks at small values of $\Delta\eta_{j1,j2}$ and falls off rapidly for larger values. The invariant mass of the leptons and the transverse mass of the W-bosons[3] become somewhat softer once the NLO QCD corrections are included. A discussion of how these distributions can be used in searches for the Higgs boson can be found in Refs. [59,60,65]. The availability of NLO QCD predictions for those distributions should, potentially, improve the reliability of such analyses since, as follows from the discussion in this paper, theoretical uncertainties are reduced considerably.

IV. CONCLUSIONS

In this paper, we computed the NLO QCD corrections to the production of a W^+W^- pair in association with two jets in hadron collisions. We only considered the QCD contribution to this process, ignoring the possibility that it can also occur through exchanges of electroweak gauge bosons. Our calculation includes the leptonic decays of W-bosons and accounts for all spin correlations exactly.

The computation of NLO QCD corrections was performed using the method of D-dimensional generalized unitarity [8,9]. Practical implementations of the generalized unitarity technique require color ordering[4]; for this reason, the presence of any colorless particle leads to additional complication since colorless particles can not be ordered. Most processes for which the NLO QCD corrections have been computed using the on-shell methods involve at most one colorless particle. The results of this paper and of Ref. [24] show that generalized unitarity methods can be efficiently used to deal with processes with a larger number of colorless particles, although the most general framework for that is yet to be understood.

We studied some phenomenology of the W^+W^-jj production at the Tevatron and the LHC, using $\sqrt{s} = 7$ TeV for the center-of-mass collision energy of the latter. We also explored the behavior of the NLO QCD cross section for $pp \to W^+W^-jj$ as a function of the center-of-mass energy at the LHC and find that, to a good approximation, the NLO cross section grows linearly with the energy of the collider. For the renormalization and factorization scales set to $\mu = M_W$ and $\mu = 2M_W$ at the Tevatron and the LHC, respectively, the radiative corrections for both colliders are moderate; in fact they are very small for collisions at 7 TeV. We show that the uncertainty in the theoretical prediction, estimated by changing factorization and renormalization scales in the range $0.5M_W(M_W) < \mu < 2M_W(4M_W)$ at the Tevatron (LHC) is better than 10% if the NLO QCD corrections are included. Of course, at that level of precision other uncertainties—such as e.g. the imperfect knowledge of parton distribution functions—become important. We considered a number of kinematic distributions that involve lepton and jet momenta and observed that energy-related distributions ($p_\perp$, H_{TOT}) become softer once the NLO QCD corrections are included and that shapes of angular distributions are hardly affected. We also discussed the significance of $pp \to W^+W^-jj$ process as an irreducible background for the production of the Higgs boson in association with two jets at the Tevatron, as well as kinematic variables useful to disentangle a Higgs signal from the W^+W^- background.

ACKNOWLEDGMENTS

We are thankful to Keith Ellis and Zoltan Kunszt for their comments on the manuscript, and to Valentin Hirschi for useful correspondence during the preparation of this paper. This research was supported by the NSF under grant PHY-0855365, the start-up funds provided by the Johns Hopkins University and by the British Science and Technology Facilities Council, by the LHCPhenoNet network under the Grant Agreement PITN-GA-2010-264564, and by the European Research and Training Network (RTN) grant Unification in the LHC era under the Agreement PITN-GA-2009-237920. We would all like to thank CERN for hospitality while part of this work was carried out. T. M. and R. R. would also like to acknowledge the hospitality extended to them by the Particle Physics Theory Group at Johns Hopkins University, in the course of the work on this paper.

APPENDIX A: RESULTS AT A FIXED PHASE SPACE POINT

In this Appendix, we shall give numerical results for some of the tree-level, primitive and full virtual amplitudes used in this calculation. For the sake of brevity, amplitudes for some flavors and helicities are not reported here. However, we also give results for squared amplitudes, summed over helicities and color.

[3]We define $M^2_{\perp,WW} = (E_{\perp,l^+l^-} + E_{\perp,\mathrm{miss}})^2 - (\mathbf{p}_{\perp,l^+l^-} - \mathbf{p}_{\perp,\mathrm{miss}})^2$, where $E_{\perp,\mathrm{miss}} = \sqrt{\mathbf{p}^2_{\perp,\mathrm{miss}} + m^2_{l^+l^-}}$.

[4]See, however, a recent discussion in Ref. [66].

We begin by considering the process $0 \to (\bar{q}q) + (W^+ \to \nu_\mu + \mu^+) + (W^- \to e^- + \bar{\nu}_e) + g + g$, and use the phase space point defined by the following values of momenta

$$\begin{aligned}
p_1^{\bar{u}} &= (-500.00000000000000, -500.00000000000000, 0.00000000000000, 0.00000000000000),\\
p_2^{u} &= (-500.00000000000000, 500.00000000000000, 0.00000000000000, 0.00000000000000),\\
p_3^{\nu_\mu} &= (85.5312248384887, -8.22193223977868, 36.16378376820329, -77.0725048002413),\\
p_4^{\mu^+} &= (181.42881161004266, -57.85998294819373, -171.863734086635, -5.611858984813),\\
p_5^{e^-} &= (82.84930107743558, -65.90954762358915, -49.89521571962871, 5.51413360058664),\\
p_6^{\bar{\nu}_e} &= (381.47038530081545, 190.18527704151887, 292.042940984587, -155.113300136598),\\
p_7^{g} &= (54.23140701179994, -31.13301620817981, -7.9279665679114, 43.69128236111634),\\
p_8^{g} &= (214.48887016141776, -27.06079802177751, -98.519808378615, 188.59224795994947).
\end{aligned} \tag{A1}$$

Our convention for displaying four-momenta is $p = (E, p_x, p_y, p_z)$; all momenta are given in GeV.

We only include results for the case in which the helicities of the $\bar{u}u$ are $(+,-)$, even though the opposite helicities do contribute via an intermediate vector boson. We also do not include the results for $\bar{d}d$—these can be obtained by switching the order of the W-bosons and modifying the γ/Z couplings in Eq. (2.4). In Tables I, II, III, and IV, we give tree-level amplitudes as well as the ratios of the unrenormalized virtual amplitudes to the tree-level amplitudes

$$r_1 = \frac{1}{c_\Gamma}\frac{A_1}{A_0}, \qquad r_1^{[1/2]} = \frac{1}{c_\Gamma}\frac{A_1^{[1/2]}}{A_0}, \tag{A2}$$

where $c_\Gamma = \frac{\Gamma(1+\epsilon)\Gamma^2(1-\epsilon)}{(4\pi)^{2-\epsilon}\Gamma(1-2\epsilon)}$, and the renormalization scale is $\mu_R = 150$ GeV. The tree-level amplitudes A_0 are defined in Eq. (2.1), while the primitive amplitudes A_1 are defined in Eq. (2.7). The one-loop amplitudes are calculated in the four-dimensional helicity scheme [67,68]. Finally, in Table V we give the ratio

TABLE I. Numerical results for the primitive tree-level amplitude $A_0(\bar{q}_1, g_3, g_4, q_2)$, in units of 10^{-10} GeV^{-4} and the ratios of primitive one-loop amplitudes $r_1(\bar{q}_1, g_3, g_4, q_2)$.

Amplitude	$1/\epsilon^2$	$1/\epsilon$	ϵ^0
$A_0(\bar{q}_1^+, g_3^-, g_4^-, q_2^-)$			$-3.344186 + i9.912207$
$r_1(\bar{q}_1^+, g_3^-, g_4^-, q_2^-)$	-1.000000	$2.294240 - i3.141593$	$0.4601166 + i2.774496$
$A_0(\bar{q}_1^+, g_3^-, g_4^+, q_2^-)$			$0.7055311 + i6.682640$
$r_1(\bar{q}_1^+, g_3^-, g_4^+, q_2^-)$	-1.000000	$2.294240 - i3.141593$	$0.3739239 + i2.687541$
$A_0(\bar{q}_1^+, g_3^+, g_4^-, q_2^-)$			$-5.998084 - i5.572010$
$r_1(\bar{q}_1^+, g_3^+, g_4^-, q_2^-)$	-1.000000	$2.294240 - i3.141593$	$0.5484790 + i3.010535$
$A_0(\bar{q}_1^+, g_3^+, g_4^+, q_2^-)$			$-10.07279 - i3.926576$
$r_1(\bar{q}_1^+, g_3^+, g_4^+, q_2^-)$	-1.000000	$2.294240 - i3.141593$	$0.4741562 + i2.846111$

TABLE II. Numerical results for the primitive tree-level amplitude $A_0(\bar{q}_1, g_3, q_2, g_4)$, in units of 10^{-10} GeV^{-4} and the ratios of primitive one-loop amplitudes $r_1(\bar{q}_1, g_3, q_2, g_4)$.

Amplitude	$1/\epsilon^2$	$1/\epsilon$	ϵ^0
$A_0(\bar{q}_1^+, g_3^-, q_2^-, g_4^-)$			$-5.097350 + i3.386328$
$r_1(\bar{q}_1^+, g_3^-, q_2^-, g_4^-)$	-2.000000	$2.993440 + i0.000000$	$-0.07739397 + i3.420824$
$A_0(\bar{q}_1^+, g_3^-, q_2^-, g_4^+)$			$-4.426865 + i4.803504$
$r_1(\bar{q}_1^+, g_3^-, q_2^-, g_4^+)$	-2.000000	$2.993440 + i0.000000$	$6.347479 + i5.196425$
$A_0(\bar{q}_1^+, g_3^+, q_2^-, g_4^-)$			$-4.749089 + i1.306764$
$r_1(\bar{q}_1^+, g_3^+, q_2^-, g_4^-)$	-2.000000	$2.993440 + i0.000000$	$-0.8538774 + i3.373345$
$A_0(\bar{q}_1^+, g_3^+, q_2^-, g_4^+)$			$-8.206743 + i2.583236$
$r_1(\bar{q}_1^+, g_3^+, q_2^-, g_4^+)$	-2.000000	$2.993440 + i0.000000$	$6.051784 + i4.612948$

TABLE III. Numerical results for the primitive tree-level amplitude $A_0(\bar{q}_1, q_2, g_3, g_4)$, in units of 10^{-10} GeV^{-4} and the ratios of primitive one-loop amplitudes $r_1(\bar{q}_1, q_2, g_3, g_4)$.

Amplitude	$1/\epsilon^2$	$1/\epsilon$	ϵ^0
$A_0(\bar{q}_1^+, q_2^-, g_3^-, g_4^-)$			$8.441536 - i13.29854$
$r_1(\bar{q}_1^+, q_2^-, g_3^-, g_4^-)$	-3.000000	$-0.9503441 - i3.141593$	$-6.047837 - i9.654414$
$A_0(\bar{q}_1^+, q_2^-, g_3^-, g_4^+,)$			$3.721334 - i11.48614$
$r_1(\bar{q}_1^+, q_2^-, g_3^-, g_4^+)$	-3.000000	$-0.9503441 - i3.141593$	$0.9335325 - i8.464906$
$A_0(\bar{q}_1^+, q_2^-, g_3^+, g_4^-)$			$10.74717 + i4.265245,$
$r_1(\bar{q}_1^+, q_2^-, g_3^+, g_4^-)$	-3.000000	$-0.9503441 - i3.141593$	$-6.036407 - i10.58605$
$A_0(\bar{q}_1^+, q_2^-, g_3^+, g_4^+)$			$18.27953 + i1.343340$
$r_1(\bar{q}_1^+, q_2^- g_3^+, g_4^+)$	-3.000000	$-0.9503441 - i3.141593$	$0.3979266 - i9.181091$

TABLE IV. Numerical results for the primitive tree-level amplitude $A_0(\bar{q}_1, q_2, g_3, g_4)$, in units of 10^{-10} GeV^{-4} and the ratios of primitive one-loop amplitudes $r_1^{[1/2]}(\bar{q}_1, q_2, g_3, g_4)$. There are no singular contributions from these one-loop amplitudes, and swapping the gluons simply changes the sign of the amplitude.

Amplitude	ϵ^0
$A_0(\bar{q}_1^+, q_2^-, g_3^-, g_4^-)$	$8.441536 - i13.29854$
$r_1^{[1/2]}(\bar{q}_1^+, q_2^-, g_3^-, g_4^-)$	$(-0.3523178 - i4.071390) \times 10^{-2}$
$A_0(\bar{q}_1^+, q_2^-, g_3^-, g_4^+,)$	$3.721334 - i11.48614$
$r_1^{[1/2]}(\bar{q}_1^+, q_2^-, g_3^-, g_4^+)$	$0.000000 + i0.000000$
$A_0(\bar{q}_1^+, q_2^-, g_3^+, g_4^-)$	$10.74717 + i4.265245$
$r_1^{[1/2]}(\bar{q}_1^+, q_2^-, g_3^+, g_4^-)$	$0.000000 + i0.000000$
$A_0(\bar{q}_1^+, q_2^-, g_3^+, g_4^+)$	$18.27953 + i1.343340$
$r_1^{[1/2]}(\bar{q}_1^+, q_2^- g_3^+, g_4^+)$	$(-3.142652 + i1.567695) \times 10^{-2}$

TABLE V. Numerical results for the tree-level amplitude squared, in units of GeV^{-8}, and the ratio of virtual over tree-level squared amplitudes S_A summed over all helicities and colors.

Ratio	$1/\epsilon^2$	$1/\epsilon$	ϵ^0
$\sum \lvert \mathcal{A}^{\text{tree}}(\bar{d}, d, g, g)\rvert^2$			9.887737×10^{-20}
$S_A(\bar{d}, d, g, g)$	-8.666667	-2.836720	-0.6913131
$\sum \lvert \mathcal{A}^{\text{tree}}(\bar{u}, u, g, g)\rvert^2$			3.743231×10^{-20}
$S_A(\bar{u}, u, g, g)$	-8.666667	-2.786885	-4.673601

TABLE VI. Numerical results for the primitive tree-level amplitude $B_0(\bar{u}, u, \bar{c}, c)$, in units of 10^{-10} GeV^{-4} and the ratios of primitive one-loop amplitudes r_i.

Amplitude	$1/\epsilon^2$	$1/\epsilon$	ϵ^0
$B_0(\bar{u}, u, \bar{c}, c)$			$0.6391654 + i5.544406$
$r_a(\bar{u}, u, \bar{c}, c)$	-2.000000	$3.066474 + i0.000000$	$2.658086 + i2.684586$
$r_a(\bar{u}, u, c, \bar{c})$	-2.000000	$4.119961 + i0.000000$	$3.634715 + i2.090514$
$r_b(\bar{u}, u, \bar{c}, c)$	-1.000000	$2.294240 - i3.141593$	$0.1918562 + i2.854994$
$r_c(\bar{u}, u, \bar{c}, c)$	-1.000000	$-3.350152 - i3.141593$	$-3.028899 - i10.77523$
$r_d(\bar{u}, u, \bar{c}, c)$		$-0.6666667 + i0.000000$	$-2.301323 - i1.838568$

TABLE VII. Numerical results for the primitive tree-level amplitude $B_0(\bar{u}, d, \bar{s}, c)$, in units of 10^{-10} GeV^{-4} and the ratios of primitive one-loop amplitudes r_i.

Amplitude	$1/\epsilon^2$	$1/\epsilon$	ϵ^0
$B_0(\bar{u}, d, \bar{s}, c)$			$0.3350897 - i0.6484033$
$r_a(\bar{u}, d, \bar{s}, c)$	-2.000000	$3.066474 + i0.000000$	$-7.426922 - i0.3913681$
$r_a(\bar{u}, d, c, \bar{s})$	-2.000000	$4.119961 + i0.000000$	$-7.135027 - i13.92234$
$r_b(\bar{u}, d, \bar{s}, c)$	-1.000000	$2.294240 - i3.141593$	$0.7221019 + i6.182924$
$r_c(\bar{u}, d, \bar{s}, c)$	-1.000000	$-3.350152 - i3.141593$	$-7.635220 - i10.639296$
$r_d(\bar{u}, d, \bar{s}, c)$		$-0.6666667 + i0.000000$	$0.9665113 - i2.094395$

TABLE VIII. Numerical results for tree-level amplitudes squared, in units of GeV^{-8}, and the ratio of virtual over tree-level squared amplitudes S_B summed over all helicities and colors.

Ratio	$1/\epsilon^2$	$1/\epsilon$	ϵ^0
$\sum \lvert\mathcal{B}^{\text{tree}}(\bar{u}, u, \bar{c}, c)\rvert^2$			1.037139×10^{-21}
$S_B(\bar{u}, u, \bar{c}, c)$	-5.333333	7.587051	5.395242
$\sum \lvert\mathcal{B}^{\text{tree}}(\bar{u}, d, \bar{s}, c)\rvert^2$			1.123763×10^{-23}
$S_B(\bar{u}, d, \bar{s}, c)$	-5.333333	7.587051	-15.91575

$$S_A = \frac{4\pi}{\alpha_s} \frac{\sum_{\{\text{hel}\}} \text{Re}(\mathcal{A}^{\text{tree}} \mathcal{A}^{\text{1L}*})}{\sum_{\{\text{hel}\}} |\mathcal{A}^{\text{tree}}|^2}, \tag{A3}$$

where the sum is over all helicities for the quarks and gluons.

We now consider the case of $0 \to (\bar{q}q) + (W^+ \to \nu_\mu + \mu^+) + (W^- \to e^- + \bar{\nu}_e) + \bar{q}_3 + q_4$. We use the same momenta as in Eq. (A1), with the modification that the last two momenta in Eq. (A1) are now those of a $\bar{q}_3 q_4$ pair, $p_7^g \to p_7^{\bar{q}_3}$, $p_8^g \to p_8^{q_4}$. For the sake of brevity, we restrict the results given here to two sets of flavors: $\bar{u}uc\bar{c}$ and $\bar{u}d\bar{s}c$ (we are thus working with an "s-amplitude"). The flavor structure of the first set is given in Eq. (2.10). We shall also restrict ourselves to the helicities $\bar{q}q\bar{q}q = (+, -, +, -)$, although for the former set of flavors, there are four different helicity combinations that are used in the calculation. We give the ratios

$$r_i = \frac{1}{c_\Gamma} \frac{B_1^{(i)}}{B_0}, \tag{A4}$$

for $i = a, b, c, d$, where B_0 is defined in Eq. (2.9) and $B_1^{(i)}$ are defined in Eqs. (2.12), (2.13), and (2.14). The results are shown in Tables VI and VII. We also give the ratios

$$S_B = \frac{4\pi}{\alpha_s} \frac{\sum_{\{\text{hel}\}} \text{Re}(\mathcal{B}^{\text{tree}} \mathcal{B}^{\text{1L}*})}{\sum_{\{\text{hel}\}} |\mathcal{B}^{\text{tree}}|^2} \tag{A5}$$

in Table VIII.

[1] A. Denner and S. Dittmaier, Nucl. Phys. **B658**, 175 (2003).
[2] T. Binoth, J. P. Guillet, G. Heinrich, E. Pilon, and C. Schubert, J. High Energy Phys. 10 (2005) 015.
[3] A. Denner and S. Dittmaier, Nucl. Phys. **B734**, 62 (2006).
[4] R. Britto, F. Cachazo, and B. Feng, Nucl. Phys. **B725**, 275 (2005).
[5] R. Britto, F. Cachazo, and B. Feng, Phys. Lett. B **611**, 167 (2005).
[6] G. Ossola, C. G. Papadopoulos, and R. Pittau, Nucl. Phys. **B763**, 147 (2007).
[7] D. Forde, Phys. Rev. D **75**, 125019 (2007).
[8] R. K. Ellis, W. T. Giele, and Z. Kunszt, J. High Energy Phys. 03 (2008) 003.
[9] W. T. Giele, Z. Kunszt, and K. Melnikov, J. High Energy Phys. 04 (2008) 049.
[10] G. Ossola, C. G. Papadopoulos, and R. Pittau, J. High Energy Phys. 05 (2008) 004.
[11] C. F. Berger *et al.*, Phys. Rev. D **80**, 074036 (2009).
[12] C. F. Berger *et al.*, Phys. Rev. Lett. **102**, 222001 (2009).
[13] R. K. Ellis, K. Melnikov, and G. Zanderighi, Phys. Rev. D **80**, 094002 (2009).
[14] R. K. Ellis, K. Melnikov, and G. Zanderighi, J. High Energy Phys. 04 (2009) 077.

[15] K. Melnikov and G. Zanderighi, Phys. Rev. D **81**, 074025 (2010).
[16] C. F. Berger *et al.*, Phys. Rev. D **82**, 074002 (2010).
[17] A. Bredenstein, A. Denner, S. Dittmaier, and S. Pozzorini, Phys. Rev. Lett. **103**, 012002 (2009).
[18] A. Bredenstein, A. Denner, S. Dittmaier, and S. Pozzorini, J. High Energy Phys. 03 (2010) 021.
[19] G. Bevilacqua, M. Czakon, C. G. Papadopoulos, R. Pittau, and M. Worek, J. High Energy Phys. 09 (2009) 109.
[20] G. Bevilacqua, M. Czakon, C. G. Papadopoulos, and M. Worek, Phys. Rev. Lett. **104**, 162002 (2010).
[21] T. Binoth *et al.*, Phys. Lett. B **685**, 293 (2010).
[22] G. Bevilacqua, M. Czakon, A. van Hameren, C. G. Papadopoulos, and M. Worek, J. High Energy Phys. 02 (2011) 083.
[23] A. Denner, S. Dittmaier, S. Kallweit, and S. Pozzorini, Phys. Rev. Lett. **106**, 052001 (2011).
[24] T. Melia, K. Melnikov, R. Rontsch, and G. Zanderighi, J. High Energy Phys. 12 (2010) 053.
[25] T. Melia, P. Nason, R. Rontsch, G. Zanderighi, arXiv:1102.4846.
[26] C. F. Berger *et al.*, Phys. Rev. Lett. **106**, 092001 (2011).
[27] P. Mastrolia, G. Ossola, T. Reiter, and F. Tramontano, J. High Energy Phys. 08 (2010) 080.
[28] V. Hirschi, R. Frederix, S. Frixione, M. V. Garzelli, F. Maltoni *et al.*, J. High Energy Phys. 05 (2011) 044.
[29] CDF Collaboration, CDF note Report No. 9887.
[30] J. M. Campbell, R. K. Ellis, and G. Zanderighi, J. High Energy Phys. 10 (2006) 028.
[31] C. Anastasiou, G. Dissertori, M. Grazzini, F. Stockli, and B. R. Webber, J. High Energy Phys. 08 (2009) 099.
[32] E. L. Berger and J. M. Campbell, Phys. Rev. D **70**, 073011 (2004).
[33] T. Han, G. Valencia, and S. Willenbrock, Phys. Rev. Lett. **69**, 3274 (1992).
[34] T. Figy, C. Oleari, and D. Zeppenfeld, Phys. Rev. D **68**, 073005 (2003).
[35] L. J. Dixon, Z. Kunszt, and A. Signer, Nucl. Phys. **B531**, 3 (1998).
[36] L. J. Dixon, Z. Kunszt, and A. Signer, Phys. Rev. D **60**, 114037 (1999).
[37] J. M. Campbell and R. K. Ellis, Phys. Rev. D **60**, 113006 (1999).
[38] J. Ohnemus, Phys. Rev. D **44**, 3477 (1991).
[39] J. M. Campbell, K. R. Ellis, and G. Zanderighi, J. High Energy Phys. 12 (2007) 056.
[40] S. Dittmaier, S. Kallweit, and P. Uwer, Nucl. Phys. **B826**, 18 (2010).
[41] M. L. Mangano and S. J. Parke, Phys. Rep. **200**, 301 (1991).
[42] Z. Bern, L. J. Dixon, and D. A. Kosower, Nucl. Phys. **B437**, 259 (1995).
[43] Z. Bern, L. J. Dixon, and D. A. Kosower, Annu. Rev. Nucl. Part. Sci. **46**, 109 (1996).
[44] Z. Bern, L. J. Dixon, and D. A. Kosower, Nucl. Phys. **B513**, 3 (1998).
[45] R. K. Ellis, W. T. Giele, Z. Kunszt, K. Melnikov, and G. Zanderighi, J. High Energy Phys. 01 (2009) 012.
[46] F. A. Berends and W. Giele, Nucl. Phys. **B306**, 759 (1988).
[47] S. Catani and M. H. Seymour, Nucl. Phys. **B485**, 291 (1997).
[48] Z. Nagy and Z. Trocsanyi, Phys. Rev. D **59**, 014020 (1998).
[49] Z. Nagy, Phys. Rev. D **68**, 094002 (2003).
[50] J. M. Campbell and R. K. Ellis, Phys. Rev. D **62**, 114012 (2000).
[51] R. Ellis and G. Zanderighi, J. High Energy Phys. 02 (2008) 002.
[52] R. Ellis, W. T. Giele, Z. Kunszt, and K. Melnikov, Nucl. Phys. **B822**, 270 (2009).
[53] K. Melnikov and M. Schulze, Nucl. Phys. **B840**, 129 (2010).
[54] T. Binoth, M. Ciccolini, N. Kauer, and M. Kramer, J. High Energy Phys. 12 (2006) 046.
[55] B. Jager, C. Oleari, and D. Zeppenfeld, J. High Energy Phys. 07 (2006) 015.
[56] J. Alwall, P. Demin, S. de Visscher, R. Frederix, M. Herquet *et al.*, J. High Energy Phys. 09 (2007) 028.
[57] A. D. Martin, W. J. Stirling, R. S. Thorne, and G. Watt, Eur. Phys. J. C **63**, 189 (2009).
[58] CDF and D0 Collaboration, arXiv:0911.3930.
[59] J. M. Campbell, R. K. Ellis, and C. Williams, Phys. Rev. D **81**, 074023 (2010).
[60] G. Klamke and D. Zeppenfeld, J. High Energy Phys. 04 (2007) 052.
[61] G. Aad *et al.* (Atlas Collaboration), Eur. Phys. J. C **71**, 1577 (2011).
[62] V. Khachatryan *et al.* (CMS Collaboration), Phys. Lett. B **695**, 424 (2011).
[63] M. Cacciari, G. P. Salam, and G. Soyez, J. High Energy Phys. 04 (2008) 063.
[64] M. Cacciari and G. P. Salam, Phys. Lett. B **641**, 57 (2006).
[65] M. Dittmar and H. K. Dreiner, Phys. Rev. D **55**, 167 (1997).
[66] W. Giele, Z. Kunszt, and J. Winter, Nucl. Phys. **B840**, 214 (2010).
[67] Z. Bern and D. A. Kosower, Nucl. Phys. **B379**, 451 (1992).
[68] Z. Bern, A. De Freitas, L. J. Dixon, and H. Wong, Phys. Rev. D **66**, 085002 (2002).